Coincidence of Checkerboard Charge Order and Antinodal State Decoherence in Strongly Underdoped Superconducting $Bi_2Sr_2CaCu_2O_{8+\delta}$

K. McElroy,[1,2,3] D.-H. Lee,[1,2] J. E. Hoffman,[4] K. M. Lang,[5] J. Lee,[3] E. W. Hudson,[6] H. Eisaki,[7] S. Uchida,[8] and J. C. Davis[3,*]

[1]*Physics Department, University of California, Berkeley, California 94720, USA*
[2]*Material Sciences Division, Lawrence Berkeley National Lab., Berkeley, California 94720, USA*
[3]*LASSP, Department of Physics, Cornell University, Ithaca, New York 14850, USA*
[4]*Department of Applied Physics, Stanford University, Stanford, California 94305, USA*
[5]*Department of Physics, Colorado College, Colorado 80305, USA*
[6]*Department of Physics,MIT, Cambridge Massachusetts 02139, USA*
[7]*AIST, 1-1-1 Central 2, Umezono, Tsukuba, Ibaraki, 305-8568 Japan*
[8]*Department of Physics, University of Tokyo, Tokyo, 113-8656 Japan*

(Received 4 June 2004; published 18 May 2005)

The doping dependence of nanoscale electronic structure in superconducting $Bi_2Sr_2CaCu_2O_{8+\delta}$ is studied by scanning tunneling microscopy. At all dopings, the low energy density-of-states modulations are analyzed according to a simple model of quasiparticle interference and found to be consistent with Fermi-arc superconductivity. The superconducting coherence peaks, ubiquitous in near-optimal tunneling spectra, are destroyed with strong underdoping and a new spectral type appears. Exclusively in regions exhibiting this new spectrum, we find local ''checkerboard'' charge ordering of high energy states, with a wave vector of $\vec{Q} = (\pm 2\pi/4.5a_0, 0); (0, \pm 2\pi/4.5a_0) \pm 15\%$. Surprisingly, this spatial ordering of high energy states coexists harmoniously with the low energy Bogoliubov quasiparticle states.

DOI: 10.1103/PhysRevLett.94.197005 PACS numbers: 74.25.Dw, 71.18.+y, 74.50.+r, 74.72.Hs

How the electronic structure evolves with doping from a Mott insulator into a d-wave superconductor is a key issue in understanding the cuprate phase diagram. Recently it has become clear that states in different parts of momentum space exhibit quite different doping dependences. The Fermi arc [1] (near nodal) states of superconducting cuprates retain their coherence as doping is reduced, while the antinodal (near the edge of the 1st Brillouin zone) states diminish in coherence, eventually becoming completely incoherent at strong underdoping. Photoemission angle-resolved photoemission spectroscopy (ARPES) reveals this directly because the nodal states persist almost into the insulator [2,3] while the antinodal states rapidly become incoherent [4–8]. Bulk probes like thermal conductivity [9] and c-axis penetration depth [10] also show that Fermi-arc states survive down to the lowest superconducting dopings. Other probes such as optical transient grating spectroscopy [11], Raman scattering [12], and NMR [13] show very different scattering processes of antinodal versus nodal states throughout the underdoped regime.

Here we report on doping-dependent STM studies of $Bi_2Sr_2CaCu_2O_{8+\delta}(\mathrm{Bi}-2212)$ to explore the nature of antinodal decoherence. The local density of states (LDOS) is mapped by measuring the STM tip-sample differential tunneling conductance $g(\vec{r}, V) \equiv dI/dV|_{r,V}$ at each location $\vec{r}$ and bias voltage V. Since LDOS $(\vec{r}, E = eV) \propto g(\vec{r}, V)$, an energy-resolved $\vec{r}$-space electronic structure map is attained. The magnitude of the energy-gap Δ can also be mapped (gap map) [14,15].

Fourier transform scanning tunneling spectroscopy (FT-STS) was recently introduced to cuprate studies [16–20]. It allows the $\vec{q}$ vectors of spatial modulations in $g(\vec{r}, V)$ to be determined from the locations of peaks in $g(\vec{q}, V)$, the Fourier transform (FT) magnitude of $g(\vec{r}, V)$. This technique has the unique capability to relate the nanoscale $\vec{r}$-space electronic structure to that in $\vec{k}$ space [17].

For this study we used single Bi-2212 crystals grown by the floating zone method with the doping controlled by oxygen depletion. The samples were cleaved in cryogenic ultrahigh vacuum before immediate insertion into the STM. We acquired more than 10^6 spectra for this study.

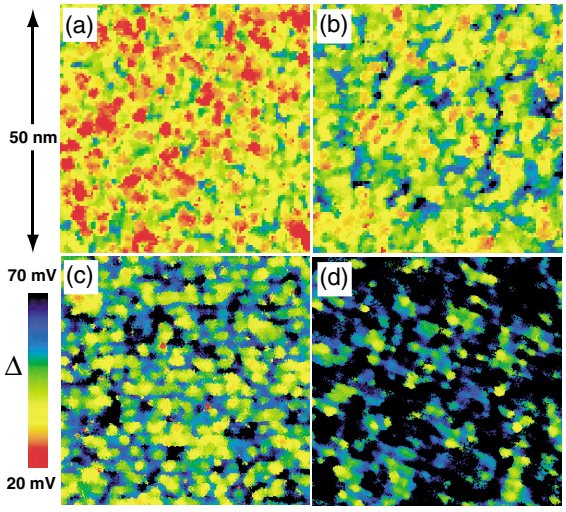

FIG. 1 (color). (a)–(d) Measured $\Delta(\vec{r})$, gap maps, for the four different hole-doping levels listed in I. Color scales identical.

TABLE I. The average properties of the samples reported.

Figure 1	T_c	p (%)	$\bar{\Delta}$ (meV)	σ meV	P_1	P_6
(a)	89K OD	19 ± 1	33 ± 1	7	30%	0%
(b)	79K UD	15 ± 1	43 ± 1	9	5%	1%
(c)	75K UD	13 ± 1	48 ± 1	10	1%	8%
(d)	65K UD	11 ± 1	>62	unclear	0%	$>55\%$

In Fig. 1 we show 50 nm square gap maps measured on samples with four different dopings. Identical color scales representing $20\ \text{meV} < \Delta(\vec{r}) < 70\ \text{meV}$ are used. The local hole concentration is impossible to determine directly. We estimate the bulk dopings in Table I. Above optimal doping [Fig. 1(a)] the vast majority of tunneling spectra are consistent with those of a $d_{x^2-y^2}$ superconductor [see Fig. 2(a) spectra 1 and 2]. However, at the lowest dopings and for gap values exceeding ~65 meV, there are many spectra where Δ is ill defined because no peaks exist at the gap edge (e.g., Fig. 2(a), spectrum 6). We represent these spectra by black in gap maps. The spatially averaged value of $\Delta(\vec{r})$, $\bar{\Delta}$, and its full width at half maximum, σ, are also in Table I. As doping is reduced, $\bar{\Delta}$ grows steadily consistent with other spectroscopic techniques, such as ARPES [21], break-junction tunneling [22], and thermal conductivity [9] which average over many nanoscale regions. There have been numerous proposals for the cause of the electronic inhomogeneity [15,23–25] but experimentally the issue is still under study.

In Fig. 2(a) we show the average spectrum of all regions exhibiting a given local gap value. They are color coded so that each gap-averaged spectrum can be associated with regions of the same color in all gap maps [Figs. 1(a)–1(d)]. This set of gap-averaged spectra is almost identical for all dopings. The changes with doping seen in $\Delta(\vec{r})$ occur because the probability of observing a given type of spectrum (1–6) in Fig. 2(a) evolves rapidly with doping

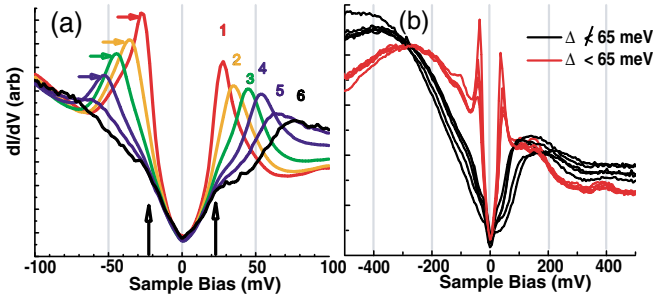

FIG. 2 (color). (a) The average spectrum, $g(E)$, associated with each gap value in a given FOV (field of view) from 1. These were extracted from 1(b) but the equivalent analysis for $g(\vec{r}, V)$ at all dopings yields results which are indistinguishable. The coherence peaks are seen spectra 1–4. (b) Characteristic spectra from the two regions $\Delta < 65$ (red) and $\Delta \not< 65$ (black). It is not the absolute scale of spectra, but changes in their shape, which is our focus.

(Table I), with P_1 and P_6 being the probability of finding spectrum 1 and 6, respectively.

Despite the intense changes with doping in the gap maps, the LDOS at energies below about $0.5\bar{\Delta}$ remains relatively homogenous for all dopings studied (black arrows in Fig. 2(a)]. These low energy LDOS do, however, exhibit numerous weak, incommensurate, energy-dispersive, LDOS modulations with long correlation lengths [16–18,20]. To explore the doping dependence of these low energy $g(\vec{r}, V)$ we use the FT-STS technique and the "octet" model [17]. Figure 3(b) [using the $\vec{q}$-vector designations in Fig. 3(a)] shows the measured length of $\vec{q}_1$, $\vec{q}_5$, and $\vec{q}_7$ as a function of energy for the three data sets. Figure 3(c) shows the locus of scattering $\vec{k}_s(E)$ [17] calculated for these three $g(\vec{r}, V)$ using

$$\vec{q}_1 = (2k_x, 0); \quad \vec{q}_5 = (0, 2k_y); \quad \vec{q}_7 = (k_x - k_y, k_y - k_x) \tag{1}$$

$$\vec{k}_s = (\pm k_x(E), \pm k_y(E)); \quad \vec{k}_s = (\pm k_y(E), \pm k_x(E)) \tag{2}$$

where k_x/k_y is the x/y component of $\vec{k}_s(E)$. These $\vec{k}_s(E)$ differ only slightly between dopings and are the same for filled and empty states.

The doping dependence of states with $\vec{k} \approx (\pm\pi/a_0, 0)$, $(0, \pm\pi/a_0)$ in the "flat band" region near the zone face

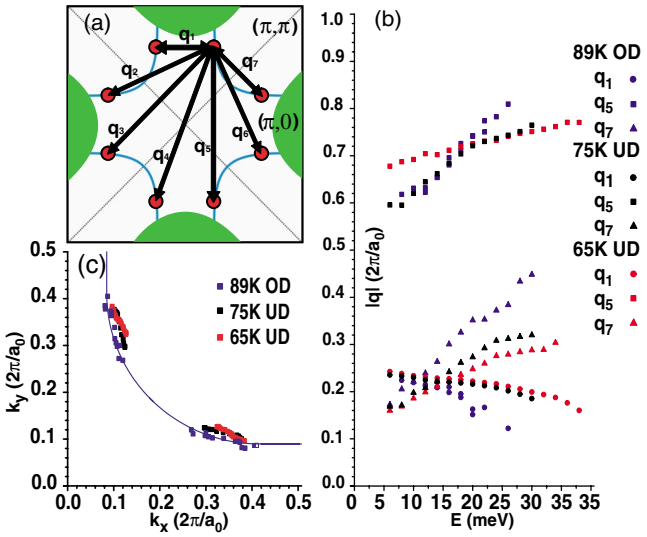

FIG. 3 (color). (a) A schematic representation of the 1st Brillouin zone and Fermi-arc location of Bi-2212. The flat-band regions near the zone face are shaded in green. The eight locations which determine the scattering within the octet model [17] (for one sub gap energy) are shown as red circles and the scattering vectors which connect these locations are show as arrows labeled by the designation of each scattering vector. (b) Measured dispersions of the LDOS modulations $\vec{q}_1$, $\vec{q}_5$, and $\vec{q}_7$ for the three dopings whose gap maps are shown in Figs. 1(a), 1(c), and 1(d). (c) Calculated loci of scattering, $\vec{k}_s$ for all three dopings. For the lowest doping the internal consistency of Eqs. (1) and (2) is worse than for optimal doping.

[green in Fig. 3(a)] is extremely different. By definition, the coherence peaks in $g(\vec{r}, V)$ occur at $E = \Delta(\vec{r})$. In all samples, they exhibit intense bias-symmetric intensity modulations in the LDOS, with wave vectors $\vec{G} = (\pm 2\pi/a_0, 0), (0, \pm 2\pi/a_0)$. Coherence peak LDOS modulations at $\vec{q} = \vec{G}$ seem to be from umklapp scattering between $\vec{k} \approx (\pm\pi/a_0, 0), (0, \pm\pi/a_0)$ [17]. Therefore, the coherence peaks in tunneling are identified empirically with the zone-face states at $\vec{k} \approx (\pm\pi/a_0, 0), (0, \pm\pi/a_0)$, as expected. Thus we consider any regions that show clear coherence peaks plus $\vec{q} = \vec{G}$ LDOS modulations to be occupied by a canonical d-wave superconductor (dSC).

Near-optimal doping, more than 98% of any field of view (FOV) exhibits this type of coherence peaked spectrum. As the range of local values of $\Delta(\vec{r})$ increases with decreasing doping, the intensity of the $\vec{q} = \vec{G}$ coherence peak LDOS modulations becomes steadily weaker until, wherever $\Delta(\vec{r}) \not< 65$ meV, they disappear altogether. This process can be seen clearly in the gap-averaged spectra of Fig. 2(a). Wherever the coherence peaks and associated $\vec{q} = \vec{G}$ LDOS modulations are absent, a well-defined new type of spectrum is always observed. Examples of this new type of spectrum, along with those of coherence peaked dSC spectra, are shown in Fig. 2(b). The coherence peaked spectra (red) are manifestly distinct from the novel spectra (black) which have a V-shaped gap reaching up to ± 75 meV but with very different evolutions at opposite bias beyond these energies. Significantly, a very similar spectrum is observed in another very underdoped cuprate $Na_xCa_{2-x}CuO_2Cl_2$, even in the nonsuperconducting phase [26]. It therefore seems reasonable that the spectrum in Fig. 2(b) is characteristic of the electronic phase at the Zero-Temperature limit of the PseudoGap region (ZTPG).

The replacement of dSC spectra by ZTPG spectra first begins to have strong impact on averaged properties of $g(\vec{r}, V)$ and $g(\vec{q}, V)$ below about $p = 0.13$ where the fractional area covered by ZTPG spectra first exceeds $\approx 10\%$ of the FOV. No further evolution in spectral shape of the ZTPG spectrum is detected at lower dopings. Instead, a steadily increasing fractional coverage of the surface by these ZTPG spectra is observed, very little spatial variations are seen at a given doping. Our previous studies [14,16,17] were carried out at dopings $p > 0.13$ where ZTPG spectra comprise a tiny fraction of any FOV.

Next we introduce a masking process to separate the electronic structure of ZTPG nanoregions from the dSC ones. From a strongly underdoped data set [Fig. 1(d)], the $g(\vec{r}, V)$ in all regions where $\Delta(\vec{r}) \not< 65$ meV are excised and used to form a new masked data set $g(\vec{r}, V)|_{\Delta \not< 65}$. The remainder forms a second new data set $g(\vec{r}, V)|_{\Delta < 65}$. The cutoff $\Delta(\vec{r}) < 65$ meV was chosen because it represents where the coherence peaks with $\vec{q} = \vec{G}$ modulations have disappeared and are replaced by the ZTPG spectra.

FT-STS analysis of such $(g(\vec{r}, V)|_{\Delta \not< 65}, g(\vec{r}, V)|_{\Delta < 65})$ pairs shows that they exhibit dramatically different phenomena. In the $g(\vec{q}, V)|_{\Delta < 65}$, the dispersive trajectory of $\vec{q}_1$ is seen up to $E \approx 36$ meV and no other peaks in $g(\vec{q}, V)$ can be detected at any higher energy [red symbols in Fig. 4(c)]. In the $g(\vec{q}, V)|_{\Delta \not< 65}$ data, the identical dispersive $\vec{q}_1$ signal is seen below $E \approx 36$ meV but, in addition, a new nondispersive LDOS modulation appears between $E = -65$ meV and our maximum measured energy $E = -150$ meV [black symbols in Fig. 4(c)] with a wave vector $\vec{q}^* = (\pm 2\pi/4.5a_0, 0), (0, \pm 2\pi/4.5a_0) \pm 15\%$.

To identify nondispersive LDOS modulations integration over energy, which enhances static features, is often

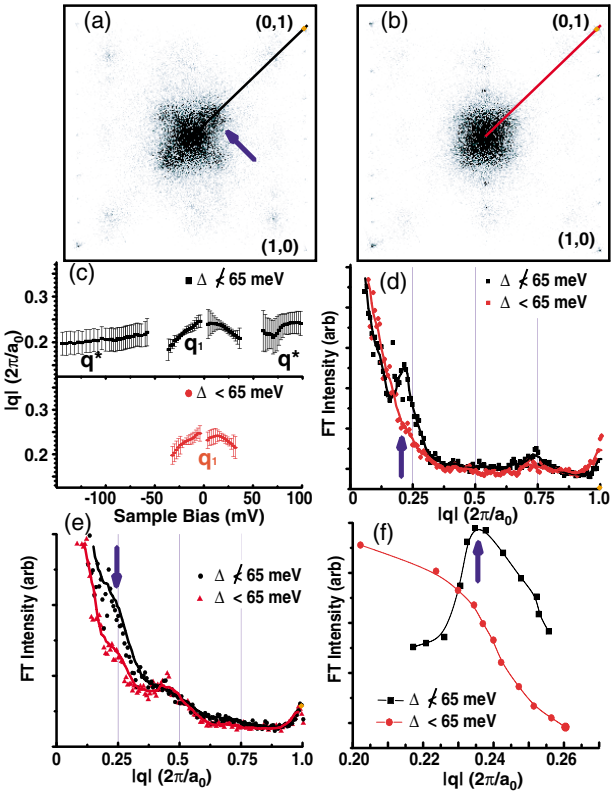

FIG. 4 (color). (a) FT of $g(\vec{r}, V)|_{\Delta \not< 65}$ integrated from $V = -65$ meV to $V = -150$ meV [taken from Fig. 1(d)]. (b) FT of the complementary, integrated $g(\vec{r}, V)|_{\Delta < 65}$. (c) Dispersion of $\vec{q}_1$ in regions with dSC coherence peaked spectra $\Delta < 65$ meV (red circles) and in regions with ZTPG spectra for $E < 36$ meV (black squares). At low energies the dispersive LDOS modulation $\vec{q}_1$ are identical in the two regions. For $E > 65$ meV, a new wave vector, $\vec{q}^*$, modulation is found only in the ZTPG regions (black). To within our uncertainty they do not disperse and $\vec{q}^* = (\pm 2\pi/4.5a_0, 0), (0, \pm 2\pi/4.5a_0) \pm 15\%$. (d) The magnitude of the integrated $g(\vec{q}, V)$ along the $\vec{q} \parallel (\pi, 0)$ direction [lines in 4(a) and 4(b)] for $\Delta \not< 65$ meV ($\Delta < 65$ meV) black (red). (e) The magnitude of the FT of the masked topographic image along the $\vec{q} \parallel (\pi, 0)$ direction for $\Delta \not< 65$ meV and ($\Delta < 65$ meV) black (red). The solid lines are guides to the eye. (f) A plot of the amplitude of the $\vec{q}_1$ LDOS modulation as a function of $|\vec{q}_1|$ for the same data set yielding Fig. 1(d). The maximum intensity of the modulations in the ZTPG regions occurs at $|\vec{q}_1| = 2\pi/4.5a_0 \pm 10\%$. No enhanced scattering of the quasiparticles in the dSC regions (red) is seen.

used [19,20]. In Fig. 4(d) we show the FT magnitude of the both components of the masked LDOS integrated over the energy range where we see $\vec{q}^*$. The ZTPG regions show a peak at the same well-defined wave vector set $\vec{q}^* = (\pm 2\pi/4.5a_0, 0), (0, \pm 2\pi/4.5a_0) \pm 15\%$ while the dSC regions show no such effect.

An even more conclusive technique for detection of net charge density variations from to nondispersive LDOS modulations is constant-current topography because it represents, albeit logarithmically, the contour of constant integrated density of states. We apply the identical mask ($\Delta \not< 65$ meV) to the topographic image acquired simultaneously with the gap map in 1(d). The magnitude of the FT along the $\vec{q} \parallel (2\pi, 0)$ for this masked topographic image shows that, in the ZTPG regions, the topography is modulated with $q_{\text{topo}} = (\pm 2\pi/4.7a_0, 0), (0, \pm 2\pi/4.7a_0) \pm 20\%$ [indicated by the arrow in Fig. 4(e)]. No such modulations at any wavelengths near this q_{topo} are found in $\Delta < 65$ meV regions [red in Fig. 4(e)].

A static charge modulation with wave vector $\vec{Q}$ should [27–29] influence quasiparticle scattering by causing an enhancement in $g(\vec{Q}, V)$ for any V. Our measurements of the intensity of the dispersive quasiparticle branch, $\vec{q}_1$, reveal a maximum in $g(\vec{q}_1, V)$ (in the ZTPG regions only) when $\vec{q}_1 = \vec{Q} = (\pm 2\pi/4.2a_0, 0), (0, \pm 2\pi/4.2a_0) \pm 15\%$ [in Fig. 4(f)]. This provides further evidence of charge order exclusively in ZPTG regions [30,31].

These observations motivate three new insights into the electronic structure of $Bi_2Sr_2CaCu_2O_{8+\delta}$. First, quasiparticle interference occurs between states in approximately the same region of $\vec{k}$ space for all dopings. These Fermi-arc states are Bogoliubov-like because they exhibit particle-hole symmetry in $\vec{k}$ space. Therefore, the Fermi-arc states are robust and gapped by superconductivity at all dopings studied. Our second finding is the very different fate of states in the flat-band regions near $\vec{k} \approx (\pm\pi/a_0, 0) \times (0, \pm\pi/a_0)$. The appearance of ZTPG spectra in strongly underdoped samples coincides with the destruction of antinodal superconducting coherence peaks. Exclusively in these ZTPG regions multiple independent phenomena with the same wave vector $\vec{Q} = \vec{q}_{\text{topo}} = \vec{q}^* = (\pm 2\pi/4.5a_0, 0), (0, \pm 2\pi/4.5a_0) \pm 15\%$ point to the appearance of an unusual charge ordered state. We refer to this as a checkerboard state because Fourier analysis of all these phenomena shows that they are symmetric under 90° rotations. The third point is that the low energy quasiparticle interference effects indicate the existence of Bogoliubov quasiparticles in *both* the ZTPG and dSC regions.

Consistent with previous deductions [1–13], we therefore find two distinct regions of $\vec{k}$ space; the Fermi arc supporting robust coherent quasiparticle states, and the antinodal region gapped by superconductivity at higher doping but becoming progressively incoherent below $p \sim 0.13$. But here we demonstrate for the first time that antinodal decoherence is coincident with the emergence of the checkerboard charge order of high energy states. Furthermore, we find that this order is not mutually exclusive with the Bogoliubov Fermi-arc states, but rather they coexist throughout the sample.

We acknowledge and thank A. V. Balatsky, S. Chakravarty, M. P. A. Fisher, T. Hanaguri, N. E. Hussey, S. Kivelson, P. A. Lee, A. Millis, D. Pines, S. Sachdev, J. Sethna, T. Uemura, A. Yazdani, J. Zaanen, and S.-C. Zhang for very helpful discussions. We acknowledge support by Grants ONR No. N00014-03-1-0674, No. NSF-ITR FDP-0205641, and ARO Grant No. DAAD 19-02-1-00-43.

*Electronic address: jcdavis@ccmr.cornell.edu

[1] M. R. Norman *et al.*, Nature (London) **392**, 157 (1998).
[2] T. Yoshida *et al.*, Phys. Rev. Lett. **91**, 027001 (2003).
[3] F. Ronning *et al.*, Phys. Rev. B **67**, 165101 (2003).
[4] A. G. Loeser *et al.*, Phys. Rev. B **56**, 14 185 (1997).
[5] A. V. Fedorov *et al.*, Phys. Rev. Lett. **82**, 2179 (1999).
[6] D. L. Feng *et al.*, Science **289**, 277 (2000).
[7] H. Ding *et al.*, Phys. Rev. Lett. **87**, 227001 (2001).
[8] X. J. Zhou *et al.*, Phys. Rev. Lett. **92**, 187001 (2004).
[9] M. Sutherland *et al.*, Phys. Rev. B **67**, 174520 (2003).
[10] A. Hosseini *et al.*, Phys. Rev. Lett. **93**, 107003 (2004).
[11] N. Gedik *et al.*, Science **300**, 1410 (2003).
[12] Y. Gallais, A. Sacuto, T. P. Devereaux, and D. Colson, Phys. Rev. B **71**, 012506 (2005).
[13] D. Pines, cond-mat/0404151.
[14] K. M. Lang *et al.*, Nature (London) **415**, 412 (2002).
[15] S. H. Pan *et al.*, Nature (London) **413**, 282 (2001).
[16] J. E. Hoffman *et al.*, Science **297**, 1148 (2002).
[17] K. McElroy *et al.*, Nature (London) **422**, 592 (2003).
[18] M. Vershinin *et al.*, Science **303**, 1995 (2004).
[19] J. E. Hoffman *et al.*, Science **295**, 466 (2002).
[20] C. Howald *et al.*, Phys. Rev. B **67**, 014533 (2003).
[21] A. Damascelli, Z. Hussain, and Z.-X. Shen, Rev. Mod. Phys. **75**, 473 (2003).
[22] N. Miyakawa *et al.*, Phys. Rev. Lett. **80**, 157 (1998).
[23] I. Martin and A. V. Balatsky, Physica (Amsterdam) **357C**, 46 (2001).
[24] D. J. Scalapino, T. S. Nunner, and P. J. Hirschfeld, cond-mat/0409204.
[25] K. H. Ahn, T. Lookman, A. Saxena, and A. R. Bishop, Phys. Rev. B **68**, 092101 (2003).
[26] T. Hanaguri *et al.*, Nature (London) **430**, 1001 (2004).
[27] D. Podolsky, E. Demler, K. Damle, and B. I. Halperin, Phys. Rev. B **67**, 094514 (2003).
[28] C.-T. Chen and N.-C. Yeh, Phys. Rev. B **68**, 220505 (2003).
[29] L. Capriotti, D. J. Scalapino, and R. D. Sedgewick, Phys. Rev. B **68**, 014508 (2003).
[30] Similar LDOS modulations have been discovered at low energies where superconductivity is destroyed leaving pseudogaplike spectra: surrounding vortex cores [19] and in the pseudogap phase above T_c [18].
[31] During review the authors have become aware of a related proposal: A. Ghosal *et al.*, cond-mat/0412241.